Role of silicon in the development of complex crystal shapes in coccolithophores

Gerald Langer[1] (iD), Alison R. Taylor[2] (iD), Charlotte E. Walker[1] (iD), Erin M. Meyer[2], Oz Ben Joseph[3] (iD), Assaf Gal[3] (iD), Glenn M. Harper[4], Ian Probert[5] (iD), Colin Brownlee[1,6] (iD) and Glen L. Wheeler[1] (iD)

[1]Marine Biological Association, The Laboratory, Citadel Hill, Plymouth, PL1 2PB, UK; [2]Department of Biology and Marine Biology, University of North Carolina Wilmington, Wilmington, NC 28403-591, USA; [3]Department of Plant and Environmental Sciences, Weizmann Institute of Science, Rehovot 7610001, Israel; [4]Plymouth Electron Microscopy Centre, University of Plymouth, Plymouth, PL4 8AA, UK; [5]FR2424 Sorbonne University / CNRS, Station Biologique de Roscoff, Roscoff 29680, France; [6]School of Ocean and Earth Science, University of Southampton, Southampton, SO14 3ZH, UK

Authors for correspondence:
Gerald Langer
Email: gerlan@mba.ac.uk

Glen L. Wheeler
Email: glw@mba.ac.uk

Summary

• The development of calcification by the coccolithophores had a profound impact on ocean carbon cycling, but the evolutionary steps leading to the formation of these complex biomineralized structures are not clear. Heterococcoliths consisting of intricately shaped calcite crystals are formed intracellularly by the diploid life cycle phase. Holococcoliths consisting of simple rhombic crystals can be produced by the haploid life cycle stage but are thought to be formed extracellularly, representing an independent evolutionary origin of calcification.
• We use advanced microscopy techniques to determine the nature of coccolith formation and complex crystal formation in coccolithophore life cycle stages.
• We find that holococcoliths are formed in intracellular compartments in a similar manner to heterococcoliths. However, we show that silicon is not required for holococcolith formation and that the requirement for silicon in certain coccolithophore species relates specifically to the process of crystal morphogenesis in heterococcoliths.
• We therefore propose an evolutionary scheme in which the lower complexity holococcoliths represent an ancestral form of calcification in coccolithophores. The subsequent recruitment of a silicon-dependent mechanism for crystal morphogenesis in the diploid life cycle stage led to the emergence of the intricately shaped heterococcoliths, enabling the formation of the elaborate coccospheres that underpin the ecological success of coccolithophores.

Introduction

Coccolithophores, unicellular pelagic algae belonging to the Haptophyta, are among the most important contributors to global carbon (C) and calcium (Ca) cycles. The acquisition of inorganic C by these algae accounts for *c.* 10% of global C fixation and has far-reaching consequences for long term C removal and sinking of organic matter (Thierstein *et al.*, 1977; Baumann *et al.*, 2004; Poulton *et al.*, 2007; Ziveri *et al.*, 2007). Coccolithophores form elaborately shaped calcite platelets called coccoliths and assemble them into a hollow coccosphere in which the cell resides. Nearly all studies of coccolithophore calcification focus on the diploid life cycle stage, which produces heterococcoliths. Although the precise function of calcification might vary between species (Monteiro *et al.*, 2016), heterococcolith formation is a highly conserved trait, suggesting that coccoliths and coccospheres are instrumental in coccolithophore ecology (Young, 1994; Bown *et al.*, 2004).

Heterococcoliths are formed in an intracellular compartment (the coccolith vesicle) and are comprised of an array of intricately shaped calcite crystals that deviate from the typical rhombohedral geometry

of inorganic calcite (Henriksen *et al.*, 2004). Coccolithophores must therefore possess regulatory mechanisms that block crystal growth in certain directions to allow precise control of crystal morphology. The ability to regulate the growth of calcite crystals in this manner was a key innovation in coccolithophore biology, allowing the formation of complex heterococcolith morphologies and distinct coccosphere architecture, such as the interlocking coccosphere of placolith-bearing species and the complex coccospheres of appendage-bearing species (Dixon, 1900; Gaarder, 1967). However, important questions remain around mechanisms that shape growing calcite crystals and the evolutionary steps that resulted in the formation of these complex biominerals.

Coccolithophores exhibit a haplo-diplontic life cycle, in which both life cycle stages can reproduce asexually and form populations with distinct spatial and seasonal distributions (Malinverno *et al.*, 2009; Cros & Estrada, 2013; D'Amario *et al.*, 2017). Whereas research attention has focused on the diploid life cycle stage, the haploid life cycle stages are broadly distributed and likely represent an important and largely overlooked aspect of coccolithophore biology (Frada *et al.*, 2018). In many species, the haploid stage may also be calcified, producing holococcoliths

that are morphologically fundamentally different from heterococcoliths (Parke & Adams, 1960; Young *et al.*, 1999; Geisen *et al.*, 2002) (Fig. 1). The abbreviations HET and HOL are used to distinguish between heterococcolith-bearing and holococcolith-bearing phases, respectively (Young *et al.*, 2003; Frada *et al.*, 2018). Holococcoliths are comprised of small calcite rhombohedra (*c.* 150 nm), which show none of the crystal shape alterations characteristic of heterococcoliths. Though holococcoliths also exhibit morphological diversity, they do not exhibit the advanced crystal morphologies of heterococcoliths. Crystal morphology is therefore a critical factor determining the overall morphology of the different coccoliths.

In comparison with heterococcolith formation, very little is known on the formation of holococcoliths. This is due in part to the absence of calcification in the haploid stage of several coccolithophore model species (e.g. *Emiliania huxleyi* and *Chrysotila carterae*, formerly *Pleurochrysis carterae*). Whereas heterococcolith formation is a wholly intracellular process, which allows precise control of nucleation and crystal growth (Young *et al.*, 1999; Brownlee *et al.*, 2015), calcite precipitation in holococcoliths has been proposed to occur extracellularly. Transmission electron microscopy (TEM) observations of HOL cultures revealed that the organic scales required as a template for holococcoliths are produced intracellularly and secreted across the plasma membrane, but no evidence was found for intracellular precipitation of calcite (Manton & Leedale, 1963; Klaveness, 1973; Rowson *et al.*, 1986). Newly formed holococcoliths appear near the base of the flagella in decalcified *Coccolithus braarudii* HOL cells, suggesting that extracellular holococcolithogenesis is restricted to the flagellar pole (Rowson *et al.*, 1986). The extracellular production of holococcoliths is supported by energy-dispersive X-ray spectroscopy (EDS) of holococcoliths that yielded estimates for magnesium (Mg) content that are much higher than heterococcoliths (Cros & Estrada, 2013), which have a low Mg content due to their intracellular site of precipitation (Stoll *et al.*, 2001). However, EDS of holococcoliths without modification of standard protocols must be viewed with caution, as their small size substantially increases the likelihood of obtaining a mixed signal from surrounding Mg-rich organic material (Stoll *et al.*, 2001).

The proposed extracellular formation of holococcoliths raises a number of unsolved issues. For example, the simple rhombic calcite crystals of holococcoliths exhibit a highly uniform shape and size. It is not clear how holococcolithophores can exert the necessary control on calcite precipitation and coccolith shape without using a confined biomineralization space (such as the coccolith vesicle in heterococcolithophores) and cytoskeletal elements to shape this space (Young *et al.*, 1999). Additionally, the very different requirements of extracellular and intracellular calcification systems suggest that fundamentally different underlying cellular mechanisms (e.g. in transport of substrates and control of calcite precipitation) are responsible for holococcolith and heterococcolith formation. Evidence from the fossil record, in which holococcoliths appear *c.* 30 million years after the first heterococcoliths (220 Ma) (Bown *et al.*, 2004), has led to suggestions that holococcolith formation represents an independent evolution of calcification that emerged after heterococcolith formation (De Vargas *et al.*, 2007). However, this evolutionary scheme appears incongruent with the lower complexity of holococcoliths compared with heterococcoliths and is considerably less parsimonious than a single common origin for calcification in coccolithophores.
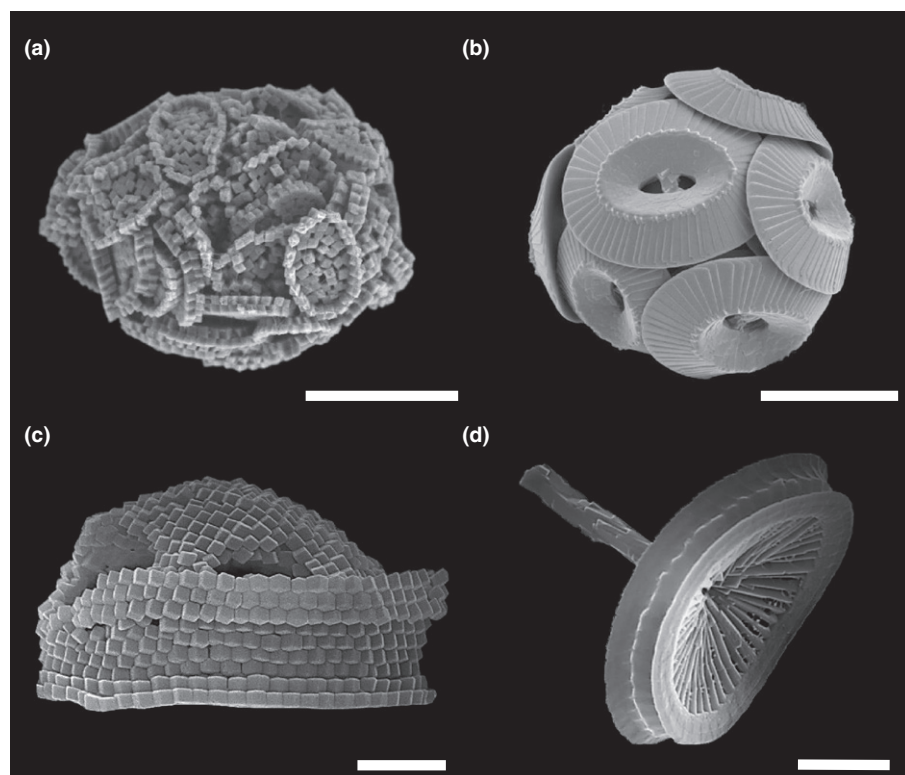

Fig. 1 Different forms of calcification between coccolithophore life cycle stages. Holococcoliths are comprised of identical rhombic crystals, whereas heterococcoliths are comprised of a variety of crystal sizes and shapes. (a) Scanning electron micrograph of *Coccolithus braarudii* holococcolith (HOL)-bearing strain (field sample, J. Young). Bar, 5 μm. (b) *Coccolithus braarudii* heterococcolith (HET)-bearing strain (field sample, J. Young). Bar, 5 μm. (c) Holococcolith from *Syracosphaera pulchra* HOL, strain RCC1461. Bar, 500 nm. (d) Heterococcolith of *S. pulchra* HET, strain RCC1460. Bar, 1 μm.

Calcification is confined to a single clade within the haptophytes, supporting a common origin (Young *et al.*, 2005; Edvardsen *et al.*, 2016). However, our current mechanistic understanding of these processes does not support a common evolutionary origin for the two modes of calcification (Frada *et al.*, 2018).

There is clearly a need to reassess the hypothesis of extracellular holococcolithogenesis, given the important evolutionary and mechanistic implications. Progress in understanding coccolithogenesis in both life cycle stages has been hindered by the lack of specific tools to disrupt the process. However, we have recently shown that certain coccolithophore species require silicon (Si) for heterococcolith formation (Durak *et al.*, 2016; Walker *et al.*, 2018). Addition of germanium (Ge), a Si analogue, led to malformed coccoliths that do not integrate into the coccosphere. Ge can therefore be used as a tool to probe heterococcolith formation, although the precise role of Si in the calcification process remains unidentified (Walker *et al.*, 2018). In this study, we present conclusive evidence for an intracellular localization of holococcolith calcite precipitation. In addition, we identify that Si contributes directly to crystal morphogenesis in heterococcoliths, but is not required for holococcolith formation. The results lead us to challenge the proposed mechanism for holococcolithophore calcification and reassess the evolution of calcification in this important group of marine calcifiers.

Materials and Methods

Culture conditions

Clonal cultures of *C. braarudii* HET (PLY182g), *Scyphosphaera apsteinii* HET (RCC1456), and *Syracosphaera pulchra* HET (RCC1460), as well as *Calyptrosphaera sphaeroidea* HOL (RCC1178, RCC1181), *Calyptrosphaera* sp. RCC6506, *C. braarudii* HOL (RCC3777, RCC1800, RCC1801), *Calcidiscus leptoporus* HOL (RCC1477), and *S. pulchra* HOL (RCC1461), were grown in aged (3 months), sterile-filtered (Stericup-GP Sterile Vacuum Filtration System, 0.22 μm pore size, polyethersulphone membrane; Merck, Gillingham, UK) natural surface seawater sampled in the English Channel off Plymouth, UK (station E1: 50°2.00′N, 4°22.00′W), enriched with 100 μM nitrate, 6.25 μM phosphate, 0.005 μM selenous acid, 0.00314 μM nickel chloride, and trace metals and vitamins as in f/2 medium (Guillard, 1975). Silicate amendments are described later. All coccolithophore strains were obtained from the Roscoff Culture Collection (http://www.roscoff-culture-collection.org), with the exception of strain PLY182g, which was obtained from the Plymouth Culture Collection (https://www.mba.ac.uk).

Coccolithophore cultures were grown under a 16 h : 8 h, light : dark cycle at a light intensity of 50–70 μmol m^{-2} s^{-1} in temperature-controlled culture rooms. All strains were grown at 15°C, with the exception of *S. apsteinii* (RCC1456) and *S. pulchra* (RCC1460, RCC1461), which were grown at 18°C. Cells were grown in dilute batch cultures, ensuring a quasi-constant seawater carbonate system over the course of the experiment (Langer *et al.*, 2013). Cell density was determined every other day (or less frequently, depending on growth rate) using a Sedgewick Rafter counting cell. Growth rate μ was calculated from an exponential regression using the natural logarithm. Growth rates were determined using triplicate cultures and error bars represent $2 \times SD$.

Specimens of the tropical benthic foraminifera *Amphistegina lessonii* were sampled from a coral reef aquarium at Burger's Zoo in Arnhem, the Netherlands. Adult specimens were kept in sterile filtered North Sea seawater (Helgoland) at 25°C, picked from the stock cultures and isolated in well plates, in which they reproduced asexually. Offspring were isolated and used for the culture experiments. The use of offspring ensured that all chambers analysed were grown under controlled experimental conditions. Juveniles (two or three chamber stage) were grown in Petri dishes to adult size. The culture medium was exchanged every other day in order to ensure quasi-constant carbonate chemistry and avoid bacterial contamination (Mewes *et al.*, 2015). Adult specimens were harvested, rinsed in reverse osmosis purified water, dried at 60°C in a drying cabinet for 24 h, and the Mg : Ca ratio was analysed by means of EDS (see later for details).

Manipulation of seawater silicon and germanium concentrations

Different batches of surface seawater with naturally low Si concentrations (ranging from 0.2 to 2 μM) collected from the English Channel (both off Plymouth, UK, and Roscoff, France) were used and amended by the addition of Si in the form of sodium metasilicate pentahydrate and Ge in the form of germanium dioxide. Seawater Si concentrations were measured using the molybdate–ascorbate assay (Zhang & Berberian, 1997), and the final concentration of Si was adjusted to 10 μM, unless stated otherwise. All Ge experiments were conducted without acclimation in pre-cultures, since Ge effects are immediate. For the low Si concentration experiment with *S. pulchra* HET (RCC1460), cells were grown in 0.2 μM Si seawater for *c.* 15 generations, sampled for scanning electron microscopy (SEM) analysis, and the remaining culture grown for a further 10 generations with the addition of 2 μM Si. The control culture was grown in the low-Si seawater batch (0.2 μM Si) with the addition of 2 μM Si.

Confocal laser scanning microscopy, decalcification, and calcein staining

Decalcification Holococcolithophores were decalcified by adding hydrochloric acid (HCl, 0.1 M) to the culture medium, which lowered the pH from 8.1 to 3. To keep the procedure as gentle as possible, cells were allowed to settle before HCl addition. After HCl addition, the culture was mixed for 20 s, and then sodium hydroxide (0.1 M) was added to restore the pH to 8.1. Cells were immediately observed by means of confocal laser scanning microscopy (CLSM) in reflected light mode (see later) to check whether they were completely decalcified. Cells were then kept under normal culturing conditions for 24 h to allow partial recalcification before CLSM imaging.

Calcein staining Well-calcified holococcolithophores were stained with 0.2 mM calcein (bis[*N*,*N*-bis(carboxymethyl)

aminomethyl]fluorescein, C0875; Sigma-Aldrich), dissolved in culture medium, for 2–3 h. The culture medium was buffered with 2 mM Hepes and adjusted to pH 8.2 to prevent holococcolith crystal dissolution (Fox *et al.*, 2018). For staining, cells were allowed to settle in a conical 15 ml tube and the culture medium was exchanged for medium containing 0.2 mM calcein. The cultures were regularly mixed during the staining period. After the staining period, the cells were washed three to five times by replacing the calcein-containing medium with normal medium. The cells were then kept under normal culturing conditions for 24 h before CLSM imaging.

Confocal laser scanning microscopy Both calcein stained and recalcifying cultures were transferred to 35 mm Petri dishes with an integrated glass coverslip and imaged using a Leica SP8 confocal microscope and Lasx (Leica, Wetzlar, Germany) application suite for acquisition and analysis. A 488 nm laser was used to excite both calcein and Chl, the emissions of which were collected at 505–565 nm and 665–750 nm, respectively. To minimize photodamage of the chloroplasts and avoid any photobleaching of the calcein-stained coccoliths, laser strength was set to ≤ 3% and photomultiplier voltages were set to 680 and 550 V for calcein and Chl channels, respectively. A pinhole of 1.5 Airy units was used with a high numerical aperture ×63 oil-immersion lens, resulting in a confocal optical thickness of 0.9 μm. For reflected light imaging of recalcifying cells, the same configuration was used except for channel 1 photomultiplier, in which a fraction of reflected 488 nm laser light was collected by setting the emission monochromator to 488–500 nm.

Transmission electron microscopy

For chemical fixation, cells were fixed in seawater (pH 8.3) containing 2.5% (v/v) glutaraldehyde and 12.5 mM Hepes for several hours, allowed to settle and resuspended in 0.1 M sodium cacodylate buffer (pH 8.6). Resuspension was repeated twice before the cells were treated with a secondary fixative of 1% osmium tetroxide in sodium cacodylate buffer (0.1 M, pH 8.6) for 1 h. The pellet of cells was rinsed twice in buffer and dehydrated in an ethanol series before embedding in Agar low-viscosity resin. The water used in the ethanol series contained 50 mM calcium chloride and was adjusted to pH 10.7 to prevent holococcolith-crystal dissolution. The hardened resin blocks were sectioned using an Ultracut E ultramicrotome (Reichert-Jung; Leica) with a Diatome diamond knife (Diatome Ltd, Nidau, Switzerland). The sections were mounted on copper grids and counterstained with a saturated solution of uranyl acetate in ethanol and Reynolds lead citrate for 15 min. The stains were adjusted to pH 10.7. Sections were examined using a Jeol 1400 EX II TEM (Jeol, Welwyn Garden City, UK) and the images captured using a Orius camera (Gatan, Abingdon, UK).

Scanning transmission electron microscopy The TEM sections were imaged using a Deben generation 5 scanning TEM (STEM) detector, and the EDS Ca maps were produced using Aztec (Oxford Instruments, Abingdon, UK).

For preserving holococcolithophore cells alongside their inorganic phases, we applied the high-pressure freezing (HPF) and freeze substitution (FS) sample preparation methodology (Kadan *et al.*, 2020). Recalcifying cells were loaded to a 100 μm deep aluminium HPF disc and were rapidly vitrified using the Leica EM ICE (Leica). To substitute the water content with an organic solvent (anhydrous acetone), we used an automated FS device (EM AFS2; Leica Microsystems GmbH). The following fixatives and stains were added to the anhydrous acetone FS solution: (1) 0.2% uranyl acetate; (2) 0.2% osmium tetroxide; (3) 2% glutaraldehyde. Following FS, cells were embedded in Epon (Agar Scientific Ltd, Stansted, UK). Sectioning of 70 nm thin slices was done with an ultra-microtome (Ultracut UCT; Leica Microsystems GmbH) and a diamond knife (Ultra 45°; Diatome Ltd). To prevent dissolution of the calcite crystals in water, ethylene glycol anhydrous 99.8% (SigmaAldrich) was used while sectioning.

Energy-dispersive X-ray spectroscopy analysis of calcite magnesium content

A 1–2 ml aliquot of mid-exponential growth phase cultures for each coccolithophore species were syringe filtered onto a 13 mm 0.4 μm Isopore filter (Merck Millipore Ltd), followed by 2–4 ml of buffered Nanopure water (1 mM Hepes, pH 8.0) to remove contaminating salts. Air-dried filters were mounted on aluminium stubs with adhesive C tabs and sputter coated with 10 nm platinum–palladium (Pt–Pd). EDS analysis was performed using a Zeiss Auriga for scanning electron microscope equipped with a Bruker xFlash 5030 detector and Quantax analysis software (Bruker Nano GmbH, Berlin, Germany). For all specimens, the primary beam acceleration was 15 kV with a working distance of 8–8.5 mm. Spectra comprising 5×10^5 counts were acquired at $(3–5) \times 10^3$ cps with a dead time of 1–3%. For Iceland spar samples, spectra were collected from random points. For plankton EDS analysis, spectra were collected from a 1–2 μm diameter region of interest.

Scanning electron microscopy analysis of coccolith morphology

Samples for SEM analysis were filtered on polycarbonate filters (0.8 μm pore size), dried in a drying cabinet at 50°C for 24 h, then sputter-coated with gold–Pd using an Emitech K550 sputter-coater at the Plymouth Electron Microscopy Centre (PEMC). Scanning electron micrographs were produced with both Jeol JSM-6610LV (Jeol) and Jeol JSM-7001F instruments at PEMC. The following categories were used to describe coccolith morphology. (1) *Coccolithus braarudii*: normal, malformation type R, minor malformation, major malformation, rhomb-like malformation, rhomb malformation. A preliminary analysis showed that the percentage of incomplete coccoliths was less than 1% in all samples. Therefore, incomplete coccoliths were not accurately quantified in the final analysis. (2) *Scyphosphaera apsteinii*: normal, malformation type R, type S, malformation type T, malformation type M. (3) *Syracosphaera pulchra*: normal, minor malformation, major malformation, malformation type C. An

average of *c*. 350 coccoliths were analysed per culture flask (Langer & Benner, 2009). The methodology of coccolith categorization and counting employed here is well established and yields robust and unbiased results (Langer *et al.*, 2013).

Analysis of *SITL* gene expression in *Coccolithus braarudii*

RNA extraction and complementary DNA synthesis A 20 ml sample of exponential growth phase culture (*c*. 20 000 cells ml^{-1}) was centrifuged at 3800 g for 5 min at 4°C. The supernatant was removed and discarded. Cell pellets were stored at −80°C before extraction. Total RNA was extracted using a Bioline Isolate II RNA Mini Kit (Meridian Bioscience, London, UK), as per manufacturer's cell culture extraction instructions with an additional elution stage to improve RNA yield. Extractions were treated with RQ1 RNase-free DNase (Qiagen) to remove any DNA contamination. Extractions were subsequently checked for purity using a Nanodrop 1000 (Thermo Fisher Scientific, Loughborough, UK) ($A_{260}/A_{280} > 1.80$) and quantified using a Quantifluor Single-tube RNA System (Promega) and a 100 ng µl^{-1} standard. A 50 ng sample of complementary DNA (cDNA) was synthesized per sample/standard using a Bioline SensiFAST cDNA Synthesis Kit (Meridian Bioscience) as per instructions with additional no reverse-transcriptase controls (NRTCs) for each treatment to ensure no DNA contamination occurred. cDNA and NRTCs were stored at −20°C before analysis.

Quantitative PCR analysis of SITL expression Primers were designed to target the *C. braarudii* genes *SITL*, *EFL*, and *RPS1* using the *C. braarudii* transcriptome (MMETSP0164) from the Marine Microbial Eukaryote Transcriptome Sequencing Project (Keeling *et al.*, 2014; Supporting Information Table S1). Reactions were conducted using a Rotorgene 6000 cycle (Qiagen) in 10 or 20 µl reaction volumes of a Bioline SensiFAST No-ROX Kit (Meridian Bioscience). Following primer optimization, PCR reactions were conducted with 400 nM final primer concentration for EFL reactions and 200 nM final concentrations for SITL and RPS1 reactions. PCR cycles were conducted with 95°C 2 min hold, followed by 40 cycles of 95°C denaturing for 5 s, 62°C annealing for 10 s and 72°C extension step (acquisition at end of extension step) for 20 s. A high-resolution melt curve, 72–95°C with 1°C ramp was conducted after amplification to ensure the amplicon had a comparable melting temperature when compared to positive control. NRTCs and no template controls were included in all reactions. All standards, samples, and controls were run in duplicate. All qPCR reaction efficiencies were > 90%, and all PCR products were run on gel electrophoresis to ensure correct amplicon size. Data were analysed using relative expression software tool REST© (Pfaffl *et al.*, 2002) and SIGMAPLOT v.13.0.

Results

Holococcoliths are produced intracellularly

Definitive evidence for the site of calcite precipitation in holococcolith formation is currently lacking. We therefore used confocal microscopy in reflectance mode to observe the appearance of extracellular holococcoliths in decalcified *C. braarudii* HOL cells. The small size and low volume of calcite in individual holococcoliths meant that we were unable to identify intracellular holococcoliths by these methods. We found that newly formed holococcoliths are observed at the flagellar pole 7–24 h after decalcification (Fig. 2a,b). To confirm whether newly formed holococcoliths appeared by the flagellar pole in cells with an intact coccosphere, we conducted calcein pulse–chase experiments (Fox *et al.*, 2018). Unstained holococcoliths appeared around the flagellar pole, showing that this is also the location where newly formed holococcoliths are integrated into the coccosphere (Fig. 2c,d). Observations of HOL strains from other species (*Calyptrosphaera* sp. and *S. pulchra*) revealed similar patterns of holococcolith formation (Fig. S1).

These observations suggest that holococcoliths are either produced via extracellular precipitation of calcite in a specialized area around the flagellar pole or are formed intracellularly and exclusively exocytosed in this region. Previous TEM studies of holococcolithogenesis in *C. braarudii* revealed no evidence of intracellular crystals (Manton & Leedale, 1963; Klaveness, 1973; Rowson *et al.*, 1986). However, the processing steps during chemical fixation for TEM can lead to a loss of calcite. We found that the small extracellular holococcolith crystals are readily dissolved compared with the bulky heterococcolith crystals when using standard TEM sample preparation protocols (Rowson *et al.*, 1986; Taylor *et al.*, 2007). A further consideration is the nature of holococcolithogenesis. Whereas heterococcolithogenesis is a lengthy process that takes up to 1–3 h (Taylor *et al.*, 2007), holococcoliths are formed rapidly, as evidenced from our live cell imaging. Thus, the rapid nature of holococcolith crystal growth combined with dissolution of holococcolith crystals during processing may make it difficult to identify intracellular holococcoliths.

We therefore developed a modified TEM sample preparation protocol for *C. braarudii* HOL that aimed to preserve calcite (see Materials and Methods section). Actual calcite crystals are rarely observed in TEM sections because sectioning often causes them to fall out. However, the crystals leave behind characteristic holes in the resin with identical dimensions to the crystals (this is also observed very clearly with TEM of heterococcoliths). In all samples, we observed holes in the resin that corresponded to extracellular holococcoliths, indicating that our modified chemical fixation did not result in calcite dissolution. Importantly, we were also able to observe that holes in the resin, representing fully formed crystals, were present on the organic scales in vesicles within the cell (Fig. 3a). The dimensions of the intracellular crystals were identical to those seen in the extracellular holococcoliths. In addition to the crystal-shaped holes in the resin, we were also able to observe actual crystals, both intra and extracellularly. We therefore performed STEM analyses of Ca distribution in these TEM sections. These analyses indicated that the extracellular and intracellular crystals were strongly enriched in Ca relative to the surrounding areas of the cell, confirming that the crystals are indeed minerals containing Ca as the major cation (Fig. 3b).
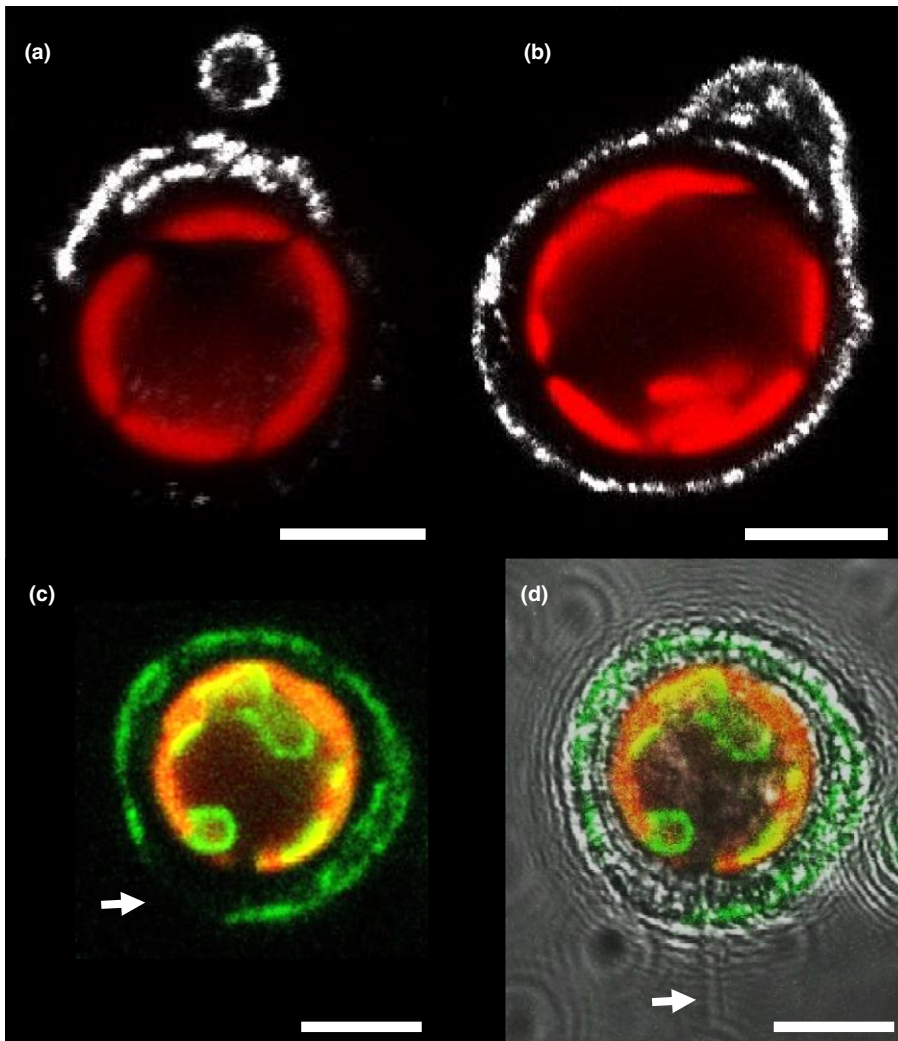
Fig. 2 Live cell imaging of holococcolith formation. (a) Confocal image of holococcolith formation in *Coccolithus braarudii* holococcolith (HOL)-bearing strain RCC3777 24 h after decalcification. Newly formed holococcoliths are viewed by reflectance (white); Chl autofluoresence is shown in red. (b) A representative cell imaged 72 h after decalcification. (c) *Coccolithus braarudii* HOL strain RCC3777 viewed 24 h after staining with calcein (green). Newly formed coccoliths are not stained, leading to a gap in the calcein staining of the coccosphere (arrow). (d) Overlay of transmitted-light image indicating the presence of an intact coccosphere and the position of the haptonema (arrow). Bars, 5 μm.

HPF followed by FS with a resin is an alternative to chemical fixation methods for TEM that is less likely to lead to calcite dissolution or loss (Kadan *et al.*, 2020). Such sample preparation of *C. sphaeroidea* HOL revealed that calcite crystals were present in an intracellular vesicle associated with the Golgi apparatus (Fig. 3c). Importantly, whilst many crystals were observed as holes in the resin, we were again able to observe intact calcite crystals, both intra and extracellularly. Taken together, our data demonstrate that holococcolith crystals in both species are formed within an intracellular coccolith vesicle, in a manner highly similar to heterococcolith formation. As many of the *C. braarudii* HOL and *C. sphaeroidea* HOL cells observed possessed intracellular organic scales that were not calcified, we propose that the small holococcolith crystals may be precipitated shortly before secretion.

Holococcoliths have a low magnesium content

Heterococcoliths have a characteristically low Mg content, which is likely due to the ability of the cell to restrict entry of Mg into the coccolith vesicle (Stoll *et al.*, 2001). We therefore performed an extensive EDS analysis of *C. braarudii* and *C. leptoporus*

heterococcolith and holococcoliths, using a modified protocol to prevent contaminating signals from the residual cellular material and substrate around the coccoliths. We found that both holo and heterococcoliths have a very low Mg content (below the limit of detection for EDS), characteristic of intracellular precipitation (Fig. 4; Table S2). This contrasts with the much higher Mg content of the calcified test of foraminifera, which are produced in a confined extracellular space (Spindler & Roettger, 1973). The low Mg content of holococcoliths supports the hypothesis that holococcolithogenesis and heterococcolithogenesis utilize the same cellular route for Ca^{2+} transport. We therefore conclude that holococcoliths, as with heterococcoliths, are formed in intracellular vesicles by precipitation onto an organic scale or baseplate and have a very similar chemical composition.

Holococcolithophores do not require silicon for calcification

The aforementioned findings indicate that shared cellular mechanisms likely contribute to coccolith formation in HOL and HET strains. However, there are key differences in crystal morphology between holococcoliths and heterococcoliths, indicating that additional cellular mechanisms must contribute to the complex
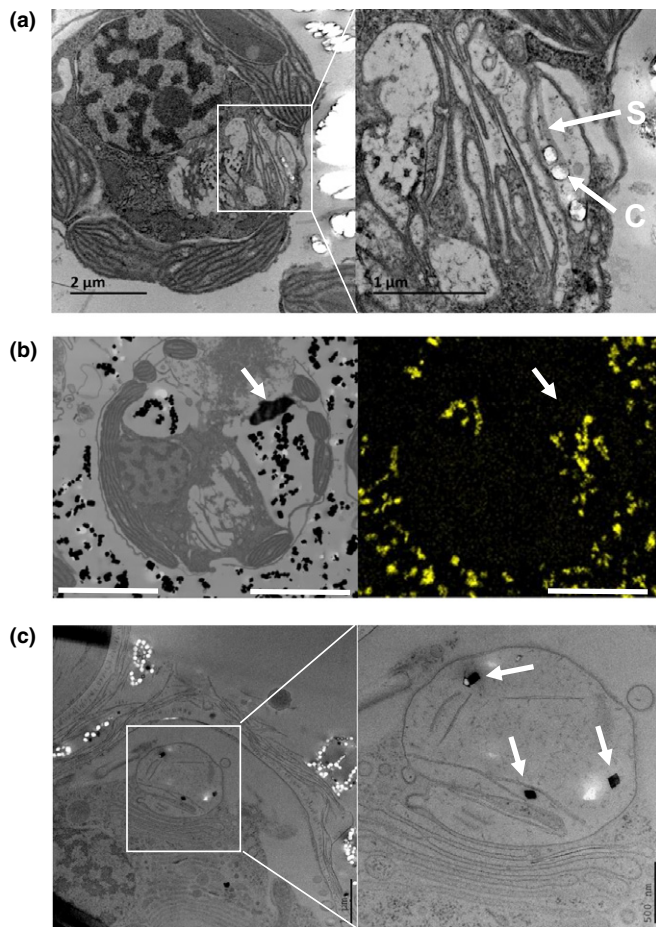
Fig. 3 Holococcolith formation occurs intracellularly. (a) Left: a transmission electron micrograph of a *Coccolithus braarudii* holococcolith (HOL; RCC3777) cell following chemical fixation. Right: expanded view of a vesicle containing a scale (S) with crystals (C) positioned on top. The position of the crystals in this image is indicated by holes in the resin. C, carbon; Ca, calcium; O, oxygen; Mg, magnesium; Pd, palladium; Pt, platinum. (b) Left: a scanning transmission electron micrograph of *C. braarudii* HOL (RCC3777) showing intact crystals as electron-dense areas, both extra- and intracellularly. Right: energy-dispersive X-ray spectroscopy (EDS) analysis indicating that a high Ca signal (yellow) is associated with the crystals. The EDS analysis therefore confirms that the crystals contain Ca as the major cation. Note that a large unidentified electron-dense area unrelated to the crystals (arrow) does not display a high Ca signal. Bars, 5 μm. (c) Left: transmission electron micrograph of a *Calyptrosphaera sphaeroidea* (RCC1181) cell that was high-pressure frozen and freeze substituted. In this image, the position of crystals appears either as electron-dense areas (intact crystals) or as holes in the resin (white). Right: expanded view of vesicle containing several scales and three intact crystals (arrows).

Fig. 4 Holococcoliths have a low magnesium (Mg) content. (a) Energy-dispersive X-ray spectroscopy (EDS) spectra showing a clearly identifiable Mg peak in the foraminifera *Amphistegina lessonii*, which calcifies extracellularly. An example of Iceland spar crystal (low-Mg calcite) is shown for comparison. Inset shows Mg peak in more detail. (b) EDS spectra of holo and heterococcoliths of *Coccolithus braarudii* (RCC3777 and PLY182g, respectively) showing very low Mg content in both. (c) EDS spectra of holo and heterococcoliths of *Calcidiscus leptoporus* heterococcolith (HET, RCC1130; HOL strain isolated directly from HET RCC1130 culture) showing equally low Mg content in both holo and heterococcoliths.

crystal morphology of heterococcoliths. To examine these mechanisms, we first determined whether holococcolithogenesis was sensitive to Ge, which has previously been used to disrupt heterococcolith formation (Durak *et al.*, 2016). In *C. braarudii* HET cells, coccolith formation is severely disrupted by a Ge : Si ratio of 0.2, and higher Ge concentrations (Ge : Si = 1.0) inhibit cell growth (Durak *et al.*, 2016; Walker *et al.*, 2018). By contrast, Ge had no discernible effect on multiple *C. braarudii* HOL strains, even at a very high Ge : Si of 10 (Figs 5a, S2). Observation of cells
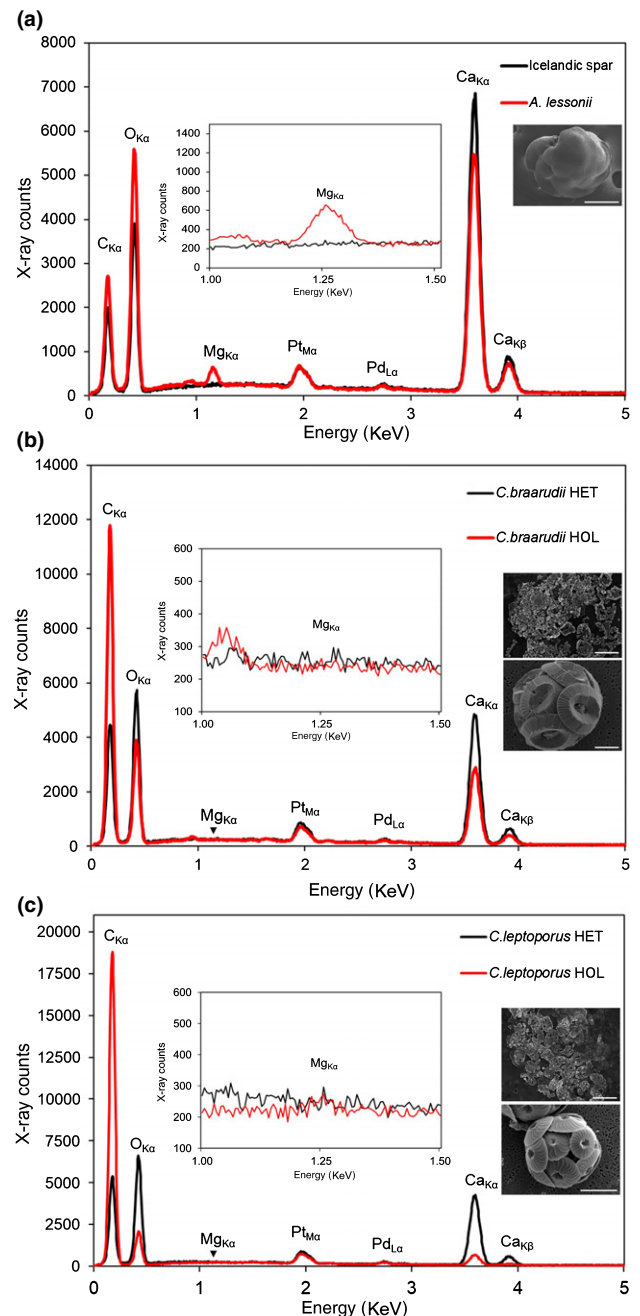
by light microscopy suggested that calcification was unaffected. The percentage of normal crystals in the Ge-treated cells was $98.4 \pm 0.5\%$, compared with $98.8 \pm 0.7\%$ in the control. Si transport in *C. braarudii* HET cells is likely mediated by a

specific Si transporter (SITL; Durak *et al.*, 2016). Quantitative reverse transcription PCR showed that the SITL transcript was not expressed in *C. braarudii* HOL cells (Fig. S3). Thus, *C. braarudii* HOL have no apparent requirement to actively transport Si across cellular membranes. These data strongly suggest that the formation of *C. braarudii* holococcoliths, unlike heterococcoliths, does not require Si.

The requirement for Si in heterococcolith formation has been lost in certain coccolithophore lineages, such as the Noelaerhabdaceae (*Emiliania/Gephyrocapsa*; Durak *et al.*, 2016). We therefore tested whether HOL strains from other species within the Coccolithales exhibited sensitivity to Ge. *Calcidiscus leptoporus* HET are Ge sensitive (Durak *et al.*, 2016), but *C. leptoporus*

Fig. 5 Holococcolithophores are largely insensitive to germanium (Ge). (a) Growth rate of different holococcolithophore strains grown under control conditions and Ge : silicon (Si) = 10. *Coccolithus braarudii*, *Calcidiscus leptoporus*, and *Calyptrosphaera* sp. holococcolith (HOL) strains grow normally even at very high Ge : Si ratios (no significant differences, *t*-test). All growth rates are means of three replicate cultures. Error bars represent ± 2SD. (b) Growth rate of *Syracosphaera pulchra* heterococcolith (HET; RCC1460) at different Ge : Si. **, *P* < 0.01, *t*-test. (c) Growth rate of *S. pulchra* HOL (RCC1461) grown under two different Ge : Si ratios (0.1 and 1). Grey bars, control; white bars, Ge treatment. *, *P* < 0.05, *t*-test. (d) Representative scanning electron microscopy images for *S. pulchra* HOLs under control conditions (left) or Ge : Si = 1.0 treatment (right). No malformations are observed in Ge-treated HOLs. Bars, 500 nm.

HOL grew and calcified normally at Ge : Si = 10. We also found that *Calyptrosphaera* HOL strains were insensitive to Ge (*C. sphaeroidea* RCC1178, noncalcifying) and the heavily calcifying RCC6506 (*Calyptrosphaera* sp.) (Fig. 5a), although it is not known whether HET strains for these species require Si.

We next examined the effect of Ge on calcification in a member of the Syracosphaerales, *S. pulchra*. The *S. pulchra* HET strain exhibited a high sensitivity to Ge, with no growth observed at Ge : Si = 0.1 (Fig. 5b). By contrast, the *S. pulchra* HOL exhibited no effect of Ge : Si = 0.1 on calcification and growth rate (Fig. 5c). This suggests that Si is not required for calcification in holococcoliths in Syracosphaerales. However, we did find that *S. pulchra* HOL was sensitive to much higher Ge concentrations, with no growth at Ge : Si = 10 and a lower growth rate at Ge : Si = 1.0. Importantly, the reduced growth at Ge : Si = 1.0 was not associated with a visible defect in calcification as the coccosphere remained intact and the morphology of holococcolith crystals was unaffected (Fig. 5d). The percentage of normal crystals in the Ge-treated *S. pulchra* HOL was 99.2 ± 0.3%, compared with 98.6 ± 0.9% in the control. We conclude that the sensitivity of *S. pulchra* HOL to high Ge : Si is not related to calcification and represents a nonspecific sensitivity to high Ge concentrations, as observed in other nonsilicifying and noncalcifying organisms.
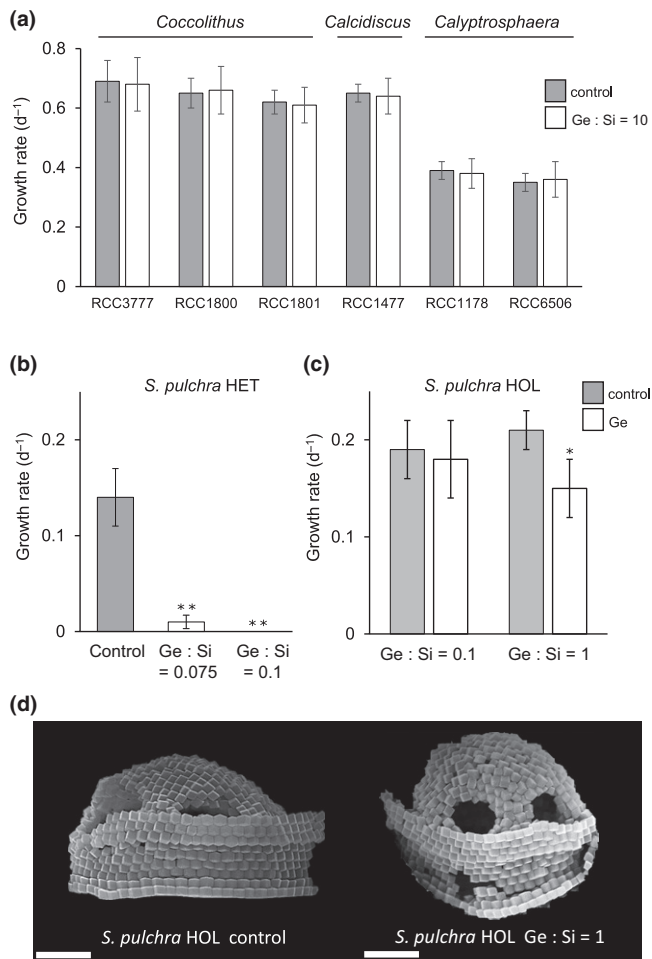
Silicon-requiring heterococcolithophores need silicon for crystal growth control

The very different sensitivities of HET and HOL strains to Ge suggest that Si plays a specific role in heterococcolith formation. We previously identified that Ge causes a 'blocky' morphology in *C. braarudii* heterococcoliths (Durak *et al.*, 2016). A more detailed analysis of the nature of the Ge-induced malformations revealed that they were distinct from those commonly observed in stock cultures or in response to phosphate limitation (Gerecht *et al.*, 2015) (Fig. 6a,b). The Ge-induced malformations were typified by individual heterococcolith elements that had a rhomb-like appearance (25.9% heterococcoliths categorized as 'rhomb-like'). We were also able to identify cases (2.0% of heterococcoliths) where the entire heterococcolith appeared as a single large rhombic crystal (coccoliths categorized as 'rhomb'). The large rhombs were only ever observed in Ge-treated cultures and had a mean diameter of 3.27 ± 0.77 µm (SD), compared with 6.34 ± 1.47 µm (SD) of rhomb-like coccoliths. The production of rhombic crystals of this scale represents an inability to control crystal shape; that is, a loss of control over crystal growth. Though a rhombic morphology is typical for inorganically grown calcite (Aquilano *et al.*, 2016), it is clear that the rhombs observed represent malformed heterococcoliths. The large rhombic crystals have a low Mg content typical of heterococcoliths, indicating intracellular formation (Fig. 6c). In addition, inorganic calcium carbonate precipitation was not observed in any untreated control HOL cultures or treated HET cultures. The findings indicate that Ge treatment can lead to a remarkable loss of control over crystal growth in heterococcolith formation.
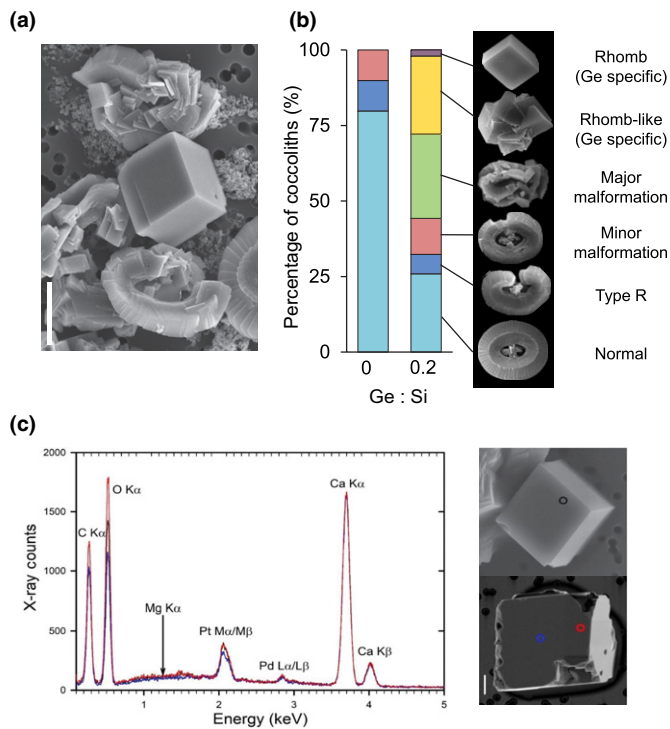
Fig. 6 Germanium (Ge) induces specific malformations in *Coccolithus braarudii* heterococcolith (HET). (a) Scanning electron microscopy (SEM) image demonstrating different coccolith malformations produced by *C. braarudii* HET (PLY182g) after treatment with Ge : silicon (Si) = 0.2 for 14 d. Bar, 4 μm. The coccolith in the centre is rhomb-shaped. (b) Quantitation of coccolith morphology of *C. braarudii* HET in response to Ge : Si = 0.2 (14 d). SEM examples illustrate the morphological categories used. Mean distribution of coccoliths is shown (*n* = 3 replicate cultures, with a minimum of 350 coccoliths counted for each replicate). (c) Three representative energy-dispersive X-ray spectroscopy (EDS) spectra from rhomb coccoliths are shown. Bar, 1 μm. C, carbon; Ca, calcium; O, oxygen; Mg, magnesium; Pd, palladium; Pt, platinum. *Coccolithus braarudii* was treated with Ge : Si = 1.0 for 24 h. The spectra were collected at the locations indicated in the SEM images (right). All EDS spectra show a low Mg content, typical of heterococcolith calcite produced intracellularly by *C. braarudii*.

Fig. 7 Disruption of silicon (Si) metabolism leads to specific malformations in *Syracosphaera pulchra* heterococcolith (HET). (a) Quantitation of coccolith morphology of *S. pulchra* HET (RCC1460) in response to Ge : Si = 0.075 (21 d). Scanning electron microscopy examples illustrate the morphological categories used. Type C malformations were observed to be specific to germanium (Ge) treatment. Mean distribution of coccoliths is shown (*n* = 3 replicate cultures, with a minimum of 350 coccoliths counted for each replicate). (b) Percentage of type C malformations observed in *S. pulchra* HET grown in control seawater (2 μM Si) or low Si (0.2 μM) for 15 generations. dSi, dissolved silicon. Low-Si cultures were then transferred to control Si for 10 generations (0.2 + 2 μM). *n* = 3 replicate cultures, error bars represent ± 2SD. **, $P < 0.01$, *t*-test. Representative type C malformations from low Si and Ge : Si = 0.075 are shown to indicate similarity.

Ge treatment also induced specific malformations in other HET strains. In *S. apsteinii* (Zygodiscales), Ge treatment resulted in the production of distinctive malformations in lopadoliths (type M), in which the distal end of the lopadolith was severely malformed (Fig. S4). Type M lopadoliths were only observed in response to Ge. As type M malformations only affect part of the coccolith, Ge appears to disrupt coccolith crystal growth rather than nucleation.

The hypothesis that Ge disturbs crystal growth control was further supported by the analysis of Ge-induced heterococcolith malformations in *S. pulchra*. We found that a specific malformation (type C) is induced by Ge (Ge : Si = 0.075) that is not observed in untreated cultures (Fig. 7a). Type C malformations also point to disturbed crystal growth control, rather than loss of nucleation control, as only some part of the coccoliths are affected. Since *S. pulchra* HET is highly sensitive to Ge, we grew this strain in low-Si seawater (15 generations) to test whether Si limitation also induces type C malformations. We found that the
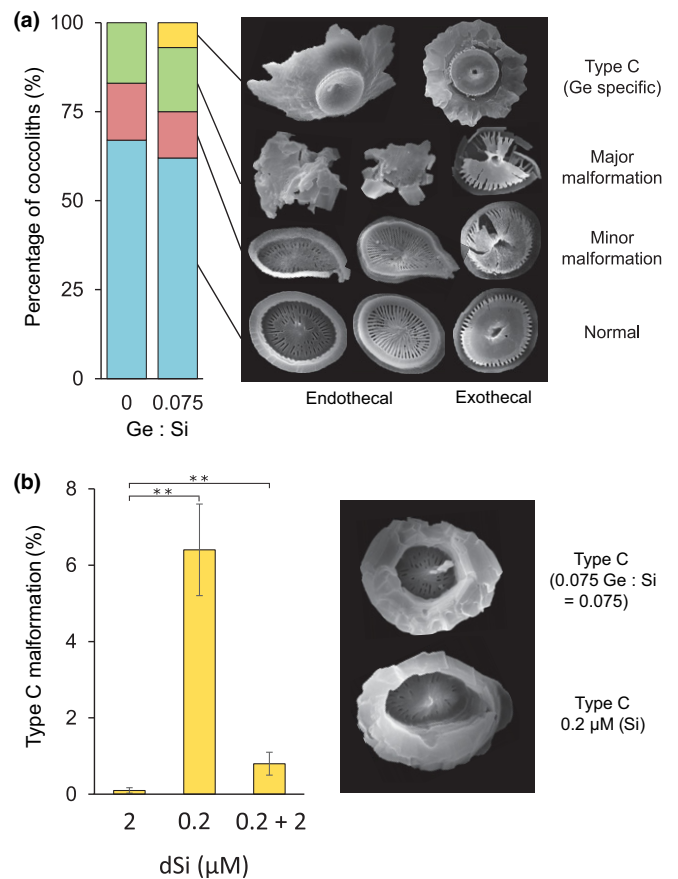
percentage of type C heterococcoliths was negligibly small at 2 μM Si (control) but increased markedly at 0.2 μM Si (Fig. 7b). Interestingly, an endothecal coccolith from *S. pulchra* exhibiting a type C malformation can be observed in a sample from northwestern Mediterranean surface water in June (Cros & Fortuno, 2002), an area where summer surface-water silicate concentrations can be very low (0.2 μM Si; Leblanc *et al.*, 2003). Natural populations of *S. pulchra* may therefore encounter Si concentrations that are sufficiently low to result in defects in calcification.

Our results demonstrate that type C malformations in *S. pulchra* HET are not due to nonspecific effects of Ge and relate specifically to Si limitation. Taken together, the effects of Ge and Si limitation on the morphology of the three species investigated support a specific role for Si in crystal growth control.

Discussion

Our analyses of the formation and elemental composition of holococcoliths strongly support the conclusion that holococcolithogenesis is an intracellular process. Although holococcolith formation was previously proposed to be extracellular, the susceptibility of holococcoliths to dissolution and their rapid generation time could easily prevent their detection by standard TEM protocols. The identification of an intracellular location for holococcolith formation resolves a number of important issues. First, it provides an explanation of how holococcolith formation is controlled through a specialized intracellular compartment that allows for precise fluid composition and potential for shaping of the holococcolith by cytoskeletal elements, as in heterococcolith formation (Wilbur & Watabe, 1963; Klaveness, 1972; Young *et al.*, 1999; Langer *et al.*, 2006). Holococcolith crystals are extremely uniform in size and shape and have a precise crystallographic orientation, which would be difficult to achieve in an unconfined extracellular space. Second, it suggests that holo and heterococcolith formation occur via similar processes and most likely involve common cellular mechanisms. Intracellular calcification requires a well-regulated pathway for transporting bicarbonate ions and Ca^{2+} into a vesicle where both the saturation state and calcite precipitation on an organic scale can be modulated. The ion transporters and the Ca-rich organelles identified in HET strains of *E. huxleyi* and *C. carterae* may therefore be common to both holo and heterococcolith formation in other species (Mackinder *et al.*, 2011; Gal *et al.*, 2017).

This conclusion has important implications not only for our understanding of the mechanisms of coccolith formation, but also for the evolution of calcification in coccolithophores. Earlier proposals that holococcoliths and heterococcoliths represent independent origins of calcification were based on the long-standing hypothesis that they are formed via fundamentally different mechanisms (De Vargas *et al.*, 2007). We must now reconsider this hypothesis, given the evidence that both are produced intracellularly. Although holococcolith formation is absent in several coccolithophore lineages (most notably *E. huxleyi* and *C. carterae*), it is likely that the last common ancestor of the Calcihaptophycidae was capable of producing both holo and heterococcoliths (Frada *et al.*, 2018). Given the similarities between the two processes, it seems likely that one form of calcification evolved from the other in this ancestor. The lower complexity of holococcoliths suggests that holococcolithogenesis may have evolved first and represents the ancestral form of calcification in coccolithophores. The additional complexity observed in heterococcolithogenesis evolved later, following the recruitment of cellular mechanisms to aid crystal morphogenesis.

Both holo and heterococcolithogenesis is a two-step process comprised of nucleation and crystal growth (Young *et al.*, 1999). Nucleation is template mediated. In both holo and heterococcolithophores, a specifically constructed template (organic scale or baseplate) is formed in a coccolith vesicle. Ions are transported into this vesicle to create a supersaturated solution, enabling nucleation. Nucleation determines the polymorph, location, and crystallographic axes orientation of the forming crystal. Initially, this crystal assumes a rhombic shape, as can be seen in the proto-coccolith ring of heterococcoliths

and the fully formed crystals of holococcoliths (Westbroek *et al.*, 1984; Young *et al.*, 1999). Holococcolithophore crystal shape is solely determined by nucleation and symmetrical rhombic crystal growth. Heterococcolith crystals, by contrast, only display rhombic morphology during the initial phase, determined by template nucleation. Later crystal shape is altered by the complex machinery, including the coccolith vesicle membrane, polysaccharides, and the cytoskeleton (Wilbur & Watabe, 1963; Klaveness, 1972; Borman *et al.*, 1982; Van der Wal *et al.*, 1983; Young *et al.*, 1999; Langer *et al.*, 2010). Our research suggests that Si plays a direct role in this process in Si-dependent species, leading to a requirement for Si in heterococcolith formation but not in holococcolith formation. The addition of Ge or limitation of Si availability has a specific impact on crystal morphogenesis but does not impact the cell's ability to precipitate calcite. The defining difference between holo and heterococcolithogenesis is therefore crystal shape modification. In other words, heterococcolithogenesis initially proceeds in exactly the same way as holococcolithogenesis, up to the point where crystal shape modification becomes relevant (Table S3).

We can therefore propose a scheme for the evolution of complex crystal morphology in heterococcolithophores (Fig. 8; Fig. S5). The last common ancestor of the Calcihaptophycidae evolved the ability to precipitate calcite within the vesicles producing organic body scales that are characteristic of this group (Eikrem *et al.*, 2016). This rudimentary form of calcification was retained in the haploid life cycle stage, but the diploid life cycle stage subsequently gained the ability to shape these calcite crystals, requiring specialized organic baseplate scales and coccolith-associated polysaccharides, allowing for the evolution of the complex morphology that defines heterococcoliths.

This evolutionary scheme is not only more parsimonious than an independent origin for holo and heterococcoliths, but also provides a stepwise progression for the increase in coccolith complexity. The hypothesis that holococcoliths evolved before heterococcoliths runs counter to evidence from the fossil record in which holococcoliths appear 37 Ma after heterococcoliths (Bown *et al.*, 2004). However, holococcoliths have a very low preservation potential compared with heterococcoliths, both in terms of their structural integrity and ability to resist dissolution (Schneidermann, 1977; Steinmetz, 1991; Ziveri *et al.*, 2000; Young *et al.*, 2005), so the fossil record of holococcoliths is likely to be relatively incomplete compared with heterococcoliths.

It should also be noted that not all extant species require Si for heterococcolith formation. Heterococcolith formation evolved *c.* 250 Ma, when surface ocean Si levels were considerably higher than at present (Marron *et al.*, 2016; Conley *et al.*, 2017). The significant decline in Si levels due to the proliferation of the diatoms, especially in the Neogene, may have driven the evolutionary loss of the Si requirement in some lineages (e.g. *Emiliania*; Durak *et al.*, 2016). Selective pressures to reduce cellular Si requirements whilst retaining the advanced features of heterococcoliths may have driven the evolution of alternative mechanisms for complex crystal morphogenesis in these lineages.
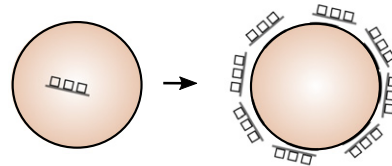
The scenario that holococcoliths evolved before heterococcoliths also raises interesting questions regarding the function of calcification. It has been argued that the primary importance of
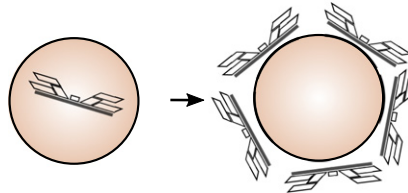
1. Noncalcified ancestor
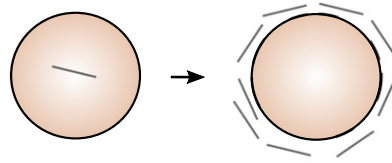
- Organic scales formed intracellularly

2. Emergence of calcified ancestor

- Intracellular formation of calcite on organic scales
- Simple rhombic crystal morphology

3. Development of heterococcoliths

- Intracellular formation of calcite on specialised organic baseplate
- Recruitment of Si-dependent mechanism allows complex crystal morphology

Fig. 8 Proposed steps in coccolith evolution. (1) The ancestor of coccolithophores likely had a covering of extracellular scales that were formed intracellularly, in a manner similar to other haptophytes. (2) Intracellular precipitation of calcite onto an organic scale enabled the formation of a calcified scale, which resembled a rudimentary holococcolith. This mechanism of calcification has been retained in the haploid life cycle stage of many extant species. (3) Subsequent development of mechanisms for crystal morphogenesis in the diploid life cycle stage resulted in the development of heterococcoliths. This was accompanied by the development of a specialized organic baseplate scale that is distinct from the organic scales.

calcification was biochemical and that the calcification process, as opposed to the product, was beneficial to the early coccolithophores (Muller, 2019). This is based on the premise that a coccosphere-centred primary function of calcification is teleological and should therefore be rejected. This, however, is not necessarily the case. It is conceivable that the first step towards a morphologically complex coccosphere was a cell covering comprised of organic scales, which might have served a protective function (Paddock, 1968; Young, 1987; Young *et al.*, 2004), albeit less so than the sturdy interlocking coccosphere of placolith-bearing species (Jaya *et al.*, 2016). The advent of calcified scales might subsequently have conferred additional properties, other than mechanical, to the cell covering (Monteiro *et al.*, 2016). For example, it has been suggested that holococcoliths can act as photonic structures that scatter ultraviolet light and therefore enable holococcolithophores to live higher in the water column (Quintero-Torres *et al.*, 2006). Though this light regulation does not necessarily require crystal shapes other than the typical calcite rhomb, other potential coccosphere functions might require special crystal shapes. The morphological diversity of holococcolithophores appears limited compared with that of heterococcolithophores (Young *et al.*, 2003). It is likely that specific functions of coccospheres require structurally complex crystals, as opposed to the simple rhombs of holococcoliths (Henriksen *et al.*, 2003). An example is the exceptional mechanical stability of the *E. huxleyi* coccosphere (Jaya *et al.*, 2016). This stability hinges mainly on the interlocking architecture of placolith-bearing coccospheres, which in turn requires complex crystal shapes that also serve to strengthen the individual coccoliths. Another example is the highly modified heterococcoliths in the appendage-bearing species *Calciopappus*, *Michaelsarsia*, and *Ophiaster*, which feature

various forms, such as whorl and link coccoliths, in a single coccosphere (Young *et al.*, 2009). Morphological specialization of heterococcoliths is also observed in the barrel-shaped lopadoliths of *S. apsteinii*, which increase in number with increasing light intensity (Drescher *et al.*, 2012). In many cases, it is not yet clear what function these elaborate structures serve, but they require highly modified coccoliths with distinct crystal shapes. We therefore propose that the evolution of complex crystals corresponded to a diversification in the functional roles of coccoliths that likely played a central role in the expansion and proliferation of the coccolithophores in modern oceans.

Author contributions

GL, GLW, CB and ART designed the study. GL, OBJ, AG, EMM, ART and GMH contributed to the study of holococcolith

formation. GL, EMM, ART and IP contributed to effect of Ge on calcification. CEW contributed to the analysis of gene expression. GL, CB, ART and GLW wrote the paper.

ORCID

Colin Brownlee (iD) https://orcid.org/0000-0001-7838-230X
Assaf Gal (iD) https://orcid.org/0000-0003-1488-1227
Oz Ben Joseph (iD) https://orcid.org/0000-0001-7670-407X
Gerald Langer (iD) https://orcid.org/0000-0002-7211-4889
Ian Probert (iD) https://orcid.org/0000-0002-1643-1759
Alison R. Taylor (iD) https://orcid.org/0000-0002-2275-0246
Charlotte E. Walker (iD) https://orcid.org/0000-0002-8570-2399
Glen L. Wheeler (iD) https://orcid.org/0000-0002-4657-1701

Data availability

Correspondence and material requests should be addressed to GLW.

References

Aquilano D, Otalora F, Pastero L, Garcia-Ruiz JM. 2016. Three study cases of growth morphology in minerals: halite, calcite and gypsum. *Progress in Crystal Growth and Characterization of Materials* **62**: 227–251.

Baumann KH, Bockel B, Frenz M. 2004. Coccolith contribution to South Atlantic carbonate sedimentation. In: Thierstein HR, Young JR, eds. *Coccolithophores: from molecular processes to global impact*. Berlin, Germany: Springer, 367–402.

Borman AH, Dejong EW, Huizinga M, Kok DJ, Westbroek P, Bosch L. 1982. The role in $CaCO_3$ crystallization of an acid Ca^{2+}-binding polysaccharide associated with coccoliths of *Emiliania huxleyi*. *European Journal of Biochemistry* **129**: 179–183.

Bown PR, Lees JA, Young JR. 2004. Calcareous nannoplankton evolution and diversity through time. In: Thierstein HR, Young JR, eds. *Coccolithophores: from molecular processes to global impact*. Berlin, Germany: Springer, 481–508.

Brownlee C, Wheeler GL, Taylor AR. 2015. Coccolithophore biomineralization: new questions, new answers. *Seminars in Cell & Developmental Biology* **46**: 11–16.

Conley DJ, Frings PJ, Fontorbe G, Clymans W, Stadmark J, Hendry KR, Marron AO, De La Rocha CL. 2017. Biosilicification drives a decline of dissolved Si in the oceans through geologic time. *Frontiers in Marine Science* **4**: e397.

Cros L, Estrada M. 2013. Holo-heterococcolithophore life cycles: ecological implications. *Marine Ecology Progress Series* **492**: 57–68.

Cros L, Fortuno JM. 2002. Atlas of northwestern Mediterranean coccolithophores. *Scientia Marina* **66**: 5–182.

D'Amario B, Ziveri P, Grelaud M, Oviedo A, Kralj M. 2017. Coccolithophore haploid and diploid distribution patterns in the Mediterranean Sea: can a haplo-diploid life cycle be advantageous under climate change? *Journal of Plankton Research* **39**: 781–794.

Dixon HH. 1900. On the structure of coccospheres and the origin of coccoliths. *Proceedings of the Royal Society* **66**: 305–315.

Drescher B, Dillaman RM, Taylor AR. 2012. Coccolithogenesis in *Scyphosphaera apsteinii* (Prymnesiophyceae). *Journal of Phycology* **48**: 1343–1361.

Durak GM, Taylor AR, Walker CE, Probert I, de Vargas C, Audic S, Schroeder D, Brownlee C, Wheeler GL. 2016. A role for diatom-like silicon transporters in calcifying coccolithophores. *Nature Communications* **7**: e10543.

Edvardsen E, Egge E, Vaulot D. 2016. Diversity and distribution of haptophytes revealed by environmental sequencing and metabarcoding – a review. *Perspectives in Phycology* **3**: 77–91.

Eikrem W, Medlin LK, Henderiks J, Rokitta SD, Rost B, Probert I, Throndsen J, Edvardsen B. 2016. Haptophyta. In: Archibald JM,

Simpson AGB, Slamovits CH, Margulis L, Melkonian M, Chapman DJ, Corliss JO, eds. *Handbook of the protists*. Cham, Switzerland: Springer International, 1–61.

Fox E, Meyer E, Panasiak N, Taylor AR. 2018. Calcein staining as a tool to investigate coccolithophore calcification. *Frontiers in Marine Science* **5**: e326.

Frada MJ, Bendif EM, Keuter S, Probert I. 2018. The private life of coccolithophores. *Perspectives in Phycology* **6**: 11–30.

Gaarder KR. 1967. Observations on the genus *Ophiaster gran* (Coccolithineae). *Sarsia* **29**: 183–192.

Gal A, Sviben S, Wirth R, Schreiber A, Lassalle-Kaiser B, Faivre D, Scheffel A. 2017. Trace-element incorporation into intracellular pools uncovers calcium-pathways in a coccolithophore. *Advanced Science* **4**: e1700088.

Geisen M, Billard C, Broerse ATC, Cros L, Probert I, Young JR. 2002. Life-cycle associations involving pairs of holococcolithophorid species: intraspecific variation or cryptic speciation? *European Journal of Phycology* **37**: 531–550.

Gerecht AC, Supraha L, Edvardsen B, Langer G, Henderiks J. 2015. Phosphorus availability modifies carbon production in *Coccolithus pelagicus* (Haptophyta). *Journal of Experimental Marine Biology and Ecology* **472**: 24–31.

Guillard RRL. 1975. Culture of phytoplankton for feeding marine invertebrates. In: Smith WL, Chanley MH, eds. *Culture of marine invertebrate animals*. New York, NY, USA: Plenum Press, 29–60.

Henriksen K, Stipp SLS, Young JR, Bown PR. 2003. Tailoring calcite: nanoscale AFM of coccolith biocrystals. *American Mineralogist* **88**: 2040–2044.

Henriksen K, Stipp SLS, Young JR, Marsh ME. 2004. Biological control on calcite crystallization: AFM investigation of coccolith polysaccharide function. *American Mineralogist* **89**: 1709–1716.

Jaya BN, Hoffmann R, Kirchlechner C, Dehm G, Schen C, Langer G. 2016. Coccospheres confer mechanical protection: new evidence for an old hypothesis. *Acta Biomaterialia* **42**: 258–264.

Kadan Y, Aram L, Shimoni E, Levin-Zaidman S, Rosenwasser S, Gal A. 2020. *In situ* electron microscopy characterization of intracellular ion pools in mineral forming microalgae. *Journal of Structural Biology* **210**: e107465.

Keeling PJ, Burki F, Wilcox HM, Allam B, Allen EE, Amaral-Zettler LA, Armbrust EV, Archibald JM, Bharti AK, Bell CJ et al. 2014. The Marine Microbial Eukaryote Transcriptome Sequencing Project (MMETSP): illuminating the functional diversity of eukaryotic life in the oceans through transcriptome sequencing. *PLoS Biology* **12**: e1001889.

Klaveness D. 1972. *Coccolithus huxleyi* (Lohmann) Kamptner. I. Morphologic investigations on the vegetative cell and the process of coccolith formation. *Protistologica* **8**: 335–346.

Klaveness D. 1973. The microanatomy of *Calyptrosphaera sphaeroidea*, with some supplementary observations on the motile stage of *Coccolithus pelagicus*. *Norwegian Journal of Botany* **20**: 151–162.

Langer G, Benner I. 2009. Effect of elevated nitrate concentration on calcification in *Emiliania huxleyi*. *Journal of Nannoplankton Research* **30**: 77–80.

Langer G, Gussone N, Nehrke G, Riebesell U, Eisenhauer A, Kuhnert H, Rost B, Trimborn S, Thoms S. 2006. Coccolith strontium to calcium ratios in *Emiliania huxleyi*: the dependence on seawater strontium and calcium concentrations. *Limnology and Oceanography* **51**: 310–320.

Langer G, de Nooijer LJ, Oetjen K. 2010. On the role of the cytoskeleton in coccolith morphogenesis: the effect of cytoskeleton inhibitors. *Journal of Phycology* **46**: 1252–1256.

Langer G, Oetjen K, Brenneis T. 2013. On culture artefacts in coccolith morphology. *Helgoland Marine Research* **67**: 359–369.

Leblanc K, Queguiner B, Garcia N, Rimmelin P, Raimbault P. 2003. Silicon cycle in the NW Mediterranean Sea: seasonal study of a coastal oligotrophic site. *Oceanologica Acta* **26**: 339–355.

Mackinder L, Wheeler G, Schroeder D, von Dassow P, Riebesell U, Brownlee C. 2011. Expression of biomineralization-related ion transport genes in *Emiliania huxleyi*. *Environmental Microbiology* **13**: 3250–3265.

Malinverno E, Triantaphyllou MV, Stavrakakis S, Ziveri P, Lykousis V. 2009. Seasonal and spatial variability of coccolithophore export production at the south-western margin of Crete (eastern Mediterranean). *Marine Micropaleontology* **71**: 131–147.

Manton I, Leedale GF. 1963. Observations on the micro-anatomy of *Crystallolithus hyalinus*. *Archiv für Mikrobiologie* **47**: 115–136.

Marron AO, Ratcliffe S, Wheeler GL, Goldstein RE, King N, Not F, de Vargas C, Richter DJ. 2016. The evolution of silicon transport in eukaryotes. *Molecular Biology and Evolution* 33: 3226–3248.

Mewes A, Langer G, Thoms S, Nehrke G, Reichart GJ, de Nooijer LJ, Bijma J. 2015. Impact of seawater Ca^{2+} on the calcification and calcite Mg/Ca of *Amphistegina lessonii*. *Biogeosciences* 12: 2153–2162.

Monteiro FM, Bach LT, Brownlee C, Bown P, Rickaby RE, Poulton AJ, Tyrrell T, Beaufort L, Dutkiewicz S, Gibbs S et al. 2016. Why marine phytoplankton calcify. *Science Advances* 2: e1501822.

Muller MN. 2019. On the genesis and function of coccolithophore calcification. *Frontiers in Marine Science* 6: e49.

Paddock TBB. 1968. A possible aid to survival of the marine coccolithophorid *Cricosphaera* and similar organisms. *British Phycological Bulletin* 3: 519–523.

Parke M, Adams I. 1960. The motile (*Crystallolithus hyalinus* Gaarder & Markali) and non-motile phases in the life history of *Coccolithus pelagicus* (Wallich) Schiller. *Journal of the Marine Biological Association of the United Kingdom* 39: 263–274.

Pfaffl MW, Horgan GW, Dempfle L. 2002. Relative expression software tool (REST©) for group-wise comparison and statistical analysis of relative expression results in real-time PCR. *Nucleic Acids Research* 30: e36.

Poulton AJ, Adey TR, Balch WM, Holligan PM. 2007. Relating coccolithophore calcification rates to phytoplankton community dynamics: regional differences and implications for carbon export. *Deep Sea Research Part II: Topical Studies in Oceanography* 54: 538–557.

Quintero-Torres R, Arago JL, Torres M, Estrada M, Cros L. 2006. Strong far-field coherent scattering of ultraviolet radiation by holococcolithophores. *Physical Review E* 74: e032901.

Rowson JD, Leadbeater BSC, Green JC. 1986. Calcium-carbonate deposition in the motile (*Crystallolithus*) phase of *Coccolithus-pelagicus* (Prymnesiophyceae). *British Phycological Journal* 21: 359–370.

Schneidermann N. 1977. Selective dissolution of recent coccoliths in the Atlantic Ocean. In: Ramsay ATS, ed. *Oceanic micropaleontology*. London, UK: Academic Press, 1009–1053.

Spindler M, Roettger R. 1973. Der Kammerbauvorgang der Großforaminifere *Heterostegina depressa* (Nummulitidae). *Marine Biology* 18: 146–159.

Steinmetz JC. 1991. Calcareous nannoplankton biocoenosis: sediment trap studies in the equatorial Atlantic, central Pacific, and Panama Basin. In: Honjom S, ed. *Ocean Biocoenosis Series No. 1*. Woods Hole Oceanogr. Inst. 85. Woods Hole, MA, USA: Woods Hole Oceanographic Institute.

Stoll HM, Encinar JR, Alonso JIG, Rosenthal Y, Probert I, Klaas C. 2000GC. A first look at paleotemperature prospects from Mg in coccolith carbonate: cleaning techniques and culture measurements. *Geochemistry Geophysics Geosystems* 2: e2000GC000144.

Taylor AR, Russell MA, Harper GM, Collins TFT, Brownlee C. 2007. Dynamics of formation and secretion of heterococcoliths by *Coccolithus pelagicus* ssp. *braarudii*. *European Journal of Phycology* 42: 125–136.

Thierstein HR, Geitzenauer KR, Molfino B. 1977. Global synchroneity of late Quaternary coccolith datum levels – validation by oxygen isotopes. *Geology* 5: 400–404.

De Vargas C, Aubry M-P, Probert I, Young J. 2007. Origin and evolution of coccolithophores: from coastal hunters to oceanic farmers. In: Falkowski P, Knoll A, eds. *Evolution of primary producers in the sea*. London, UK: Elsevier, 251–285.

Van der Wal P, Dejong EW, Westbroek P, Debruijn WC, Mulderstapel AA. 1983. Ultrastructural polysaccharide localization in calcifying and naked cells of the coccolithophorid *Emiliania huxleyi*. *Protoplasma* 118: 157–168.

Walker CE, Taylor AR, Langer G, Durak GM, Heath S, Probert I, Tyrrell T, Brownlee C, Wheeler GL. 2018. The requirement for calcification differs between ecologically important coccolithophore species. *New Phytologist* 220: 147–162.

Westbroek P, Dejong EW, Vanderwal P, Borman AH, Devrind JPM, Kok D, Debruijn WC, Parker SB. 1984. Mechanism of calcification in the marine alga *Emiliania huxleyi*. *Philosophical Transactions of the Royal Society of London Series B: Biological Sciences* 304: 435.

Wilbur KM, Watabe N. 1963. Experimental studies on calcification in molluscs and the alga *Coccolithus huxleyi*. *Annals of the New York Academy of Sciences* 109: 82–112.

Young JR. 1987. Possible functional interpretations of coccolith morphology. In: Stradner H, Perch-Nielsen K, eds. *INA Vienna Meeting 1985: Proceedings. Abhandlungen der Geologischen Bundesanstalt, Wien, vol. 39*. Vienna, Austria: Geologische Bundesanstalt, 305–313.

Young JR. 1994. Functions of coccoliths. In: Winter A, Siesser WG, eds. *Coccolithophores*. Cambridge, UK: Cambridge University Press, 63–82.

Young JR, Andruleit H, Probert I. 2009. Coccolith function and morphogenesis: insights from appendage-bearing coccolithophores of the family Syracosphaeraceae (Haptophyta). *Journal of Phycology* 45: 213–226.

Young JR, Davis SA, Bown PR, Mann S. 1999. Coccolith ultrastructure and biomineralisation. *Journal of Structural Biology* 126: 195–215.

Young JR, Geisen M, Cros L, Kleijne A, Sprengel C, Probert I, Østergaard J. 2003. *A guide to extant coccolithophore taxonomy. Journal of Nannoplankton Research Special Issue 1*. London, UK: International Nannoplankton Association, 125.

Young JR, Geisen M, Probert I. 2005. Review of selected aspects of coccolithophore biology with implications for paleobiodiversity estimation. *Micropaleontology* 51: 267–288.

Young JR, Henriksen K, Probert I. 2004. Structure and morphogenesis of the coccoliths of the CODENET species. In: Thierstein HR, Young JR, eds. *Coccolithophores: from molecular processes to global impact*. Berlin, Germany: Springer, 191–216.

Zhang JZ, Berberian GA. 1997. Determination of dissolved silicate in estuarine and coastal waters by gas segmented continuous flow colorimetric analysis. In: Arar EJ, ed. *Methods for the determination of chemical substances in marine and estuarine environmental matrices*. Washington, DC, USA: US Environmental Protection Agency, Method 266.0, 1–13.

Ziveri P, de Bernardi B, Baumann KH, Stoll HM, Mortyn PG. 2007. Sinking of coccolith carbonate and potential contribution to organic carbon ballasting in the deep ocean. *Deep Sea Research Part II: Topical Studies in Oceanography* 54: 659–675.

Ziveri P, Broerse ATC, van Hinte JE, Westbroek P, Honjo S. 2000. The fate of coccoliths at 48°N 21°W, northeastern Atlantic. *Deep Sea Research Part II: Topical Studies in Oceanography* 47: 1853–1875.

Supporting Information

Additional Supporting Information may be found online in the Supporting Information section at the end of the article.

Fig. S1 Live cell imaging of holococcolith formation.

Fig. S2 Photosynthetic efficiency of holococcolithophores following Ge treatment.

Fig. S3 SITL is not expressed in *C. braarudii* HOL.

Fig. S4 Ge induces specific malformations in *S. apsteinii* HET.

Fig. S5 Evolutionary events leading to the calcification status and Ge-sensitivity of extant coccolithophore species.

Table S1 Primer details for qPCR.

Table S2 Summary of EDS results for calcite.

Table S3 Comparison of holococcolith and heterococcolith formation in *C. braarudii*.

Please note: Wiley Blackwell are not responsible for the content or functionality of any Supporting Information supplied by the authors. Any queries (other than missing material) should be directed to the *New Phytologist* Central Office.

See also the Commentary on this article by Mock, **231**: 1663–1666.